Brain, Behavior, & Immunity - Health 42 (2024) 100890

Contents lists available at ScienceDirect

Brain, Behavior, & Immunity - Health

journal homepage: www.editorialmanager.com/bbih/default.aspx

Interleukin-18 interacts with NKCC1 to mediate brain injury after intracerebral hemorrhage

Beibei Xu [a,1], Hao Li [a,b,1], He Zheng [a], Zhongyu Gao [c], Zhigang Miao [d], Xingshun Xu [a,d,***], Hao Yang [e,**], Yi Yang [a,*]

[a] Departments of Neurology, The First Affiliated Hospital of Soochow University, Suzhou, Jiangsu, China
[b] Departments of Neurology, The Fourth Affiliated Hospital of Soochow University, Suzhou, Jiangsu, China
[c] Computer Science and Engineering, University of California Davis, One Shields Avenue, Davis, CA, 95616, USA
[d] Institute of Neuroscience, Soochow University, Suzhou, Jiangsu, China
[e] Department of Fetology, The First Affiliated Hospital of Soochow University, Suzhou, Jiangsu, China

ARTICLE INFO

Keywords:
Interleukin-18
Intracerebral hemorrhage
Brain injury
Microglia
NKCC1

ABSTRACT

Interleukin 18 (IL-18), a proinflammatory cytokine, has been implicated in various neurological disorders, including cerebrovascular disease and psychiatric disorders. In a previous study, IL-18 was observed to activate microglia and enhance the inflammatory response following intracranial hemorrhage (ICH). However, the underlying mechanism remains unclear. In the present study, we found that IL-18 and IL-18 receptor (IL-18 R) are primarily secreted by neurons during the early stages after ICH, with microglia becoming the predominant source at 12–24 h after ICH. Meanwhile, the expression level of IL-18 R increased following ICH, along with an augmentation in the binding affinity of IL-18 R to IL-18. Subsequently, the deficiency of IL-18 R mitigated neurological impairment and subsequent activation of inflammatory pathways in mice post-ICH. Moreover, our findings suggest that IL-18-induced neurological injury after ICH may be mediated by the interaction between IL18R and NKCC1. Significantly, the NKCC1 inhibitor rescued the neurologic injury after ICH. In conclusion, our study suggests that targeting the IL-18/IL-18R/NKCC1 pathway could be an effective therapeutic strategy to attenuate secondary brain injury after ICH.

1. Introduction

As a life-threatening type of stroke, intracranial hemorrhage (ICH) is characterized by high mortality and high disability (Magid-Bernstein et al., 2022). The incidence is still on the rise in Asia (Tu et al., 2023). Following the onset of ICH, the primary injury is caused by the enlargement of the hematoma, which itself induces secondary brain injury (SBI) with a series of pathophysiological changes such as neuroinflammation, excitotoxicity, and neuronal apoptosis (Tang et al., 2020). Inflammation plays a pivotal role in the pathological progression of ICH, contributing to brain damage and neurobehavioral impairment (Ding et al., 2020). Despite extensive attention from researchers in both basic and clinical studies, therapeutic strategies for mitigating SBI after cerebral hemorrhage have yet to yield effective treatments to improve the prognosis of ICH patients.

Interleukin-18 (IL-18) belongs to the IL-1 cytokine family and is considered as a proinflammatory cytokine that induces IFNγ production (Dinarello, 2001). It can specifically bind to IL-18 receptor (IL-18 R) through the crystal structure of the receptor-binding protein IL-18α chain (IL-18 Rα) to deliver pro-inflammatory signals into cells, ultimately leading to NF-κB activation (Kaplanski, 2018). Previous studies have demonstrated that activation of IL-18 signaling is associated with a variety of inflammatory pathological conditions, including asthma, osteoarthritis, vaso-proliferative diseases, psychiatric disorder, and post-stroke depression (Zhang et al., 2018; Bao et al., 2020; Sukhanov et al., 2021; Du et al., 2022; Wu et al., 2020). Meanwhile, our recent findings suggest that exogenous IL-18 can exacerbate cerebral edema and neurological deficits after cerebral hemorrhage; whereas IL-18

* Corresponding author.
** Corresponding author.
*** Corresponding author. Departments of Neurology, the First Affiliated Hospital of Soochow University, Suzhou, Jiangsu, China.
E-mail addresses: Xingshunxu@suda.edu.cn (X. Xu), yanghao.71_99@yahoo.com (H. Yang), 13656229395@163.com (Y. Yang).
[1] Beibei Xu and Hao Li contributed equally.

https://doi.org/10.1016/j.bbih.2024.100890
Received 18 June 2024; Received in revised form 13 September 2024; Accepted 5 October 2024
Available online 18 October 2024

knockdown ameliorates the inflammatory response and improves neurobehavioral scores by reducing microglia activation (Li et al., 2022). However, the specific mechanism of the IL-18/IL-18 R signaling pathway remains unclear.

In this study, we examined the alternation of IL-18/IL-18 R and explored the possible mechanisms in the development of neuroinflammation following ICH.

2. Materials and methods

2.1. Reagents

IL-18 antibody (10663-1-AP; 1:1500; RRIDs: AB_2123636) was obtained from Proteintech (Wuhan, China). IL-18 R antibody (PA5-102647; 1:1500; RRIDs: AB_2852044) was obtained from Invitrogen (Carlsbad, CA, USA). NKCC1 antibody (ab303518; 1:1500; RRIDs: AB_3094810) was obtained from Abcam company (Cambridge, MA, USA). NeuN antibody (66836-1-Ig; 1:2000; RRIDs: AB_2882179) was obtained from Proteintech (Wuhan, China). Anti-Glial Fibrillary Acidic Protein Antibody (MAB360; 1:2000; RRIDs: AB_11212597) was obtained from Millipore Sigma (Boston, MA, USA). Iba1 antibody (019–19741; 1:500; RRIDss: AB_839,504) was obtained from FUJIFILM Wako Pure Chemical Corporation (Japan). TLR4 antibody (30400-1-AP; 1:2000; RRIDs: AB_3086308) was obtained from Proteintech (Wuhan, China). TRAF6 antibody (R1311-2; 1:1000; RRIDs: AB_3073257) and NF-κB p65 antibody (ET1603-12; 1:1000; RRIDs: AB_3069668) were obtained from HUABIO (China). GAPDH Mouse Monoclonal Antibody (AF0006; 1:10,000; RRIDs: AB_2715590) and β-Actin Mouse Monoclonal Antibody (AF5001; 1:10,000; RRIDs: AB_3094825) were obtained from Beyotme company (China). Histone H3 Mouse Monoclonal Antibody (YM3038; 1:5000; RRIDs: AB_3096370) was obtained from ImmunoWay (CA, USA). Secondary antibodies for Western blot analysis, including anti-rabbit IgG-HRP (7074s; 1:1000; RRIDs: AB-2099233) and anti-mouse IgG-HRP (7076s; 1:1000; RRIDs: AB-330924), were purchased from Cell Signaling Technology (Danvers, MA, USA). The Rabbit-Mouse Universal Secondary Antibody (AFIHC001) and Fluorescent Staining Kit for Immunofluorescence (AFIHC023) was obtained from AIFang biological Co., (Wuhan, China).

2.2. Animals

Adult male C57BL/6 mice (20–27 g, 8–10 weeks old) were procured from Shanghai SLAC Laboratory Animal Co., Ltd (Shanghai, China). Given the protective role of estrogen in cerebral injury and stress, this study exclusively used male mice. Male mice were provided ad libitum access to standard rodent chow and water, and were housed under controlled conditions (12 h/12 h light/dark cycle with humidity maintained between 40 and 70%, and temperature set at 23 ± 3 °C). Adult male C57BLJ/6 mice were maintained in groups of 3–4 animals per cage.

The study strictly adhered to the guidelines outlined in the National Institutes of Health guide for the care and use of laboratory animals (NIH Publications No. 8023, revised 2011). The animal experiments were conducted in compliance with the ARRIVE (Animal Research: Reporting in vivo Experiments) guidelines, with utmost efforts made to minimize animal suffering and reduce the number of animals used (Kilkenny et al., 2011). Ethical approval for all experimental procedures was granted by the Ethics Committee of the First Affiliated Hospital of Soochow University.

2.3. Experimental design

In the first part, we examined the secretion and expression of IL-18/IL-18 R. Male C57BL/6 mice was used for immunofluorescent (IF) analysis at 12 h, 24 h, and 3 d (n = 3 assigned per time point) after ICH, the sham group as control. Mice were also used for western blotting (WB), immunoprecipitation (IP) analysis, and RT-PCR analysis at 6 h, 12 h, 24 h, 3 d, and 7 d (n = 6 assigned per time point) after ICH, the sham group as control; 10 mice in each group (ICH and sham) were subjected to behavioral tests. Subsequently, we used IL-18 binding proteins (IL-18BP) to block endogenous IL-18. In this part, mice were randomly divided into four groups (n = 13), including Sham + PBS group, Sham + IL-18BP group, ICH + PBS group, and ICH + IL-18BP group. At 24 h after ICH, three mice in each group were subjected to MRI; 10 mice in each group were subjected to behavioral tests. We then cultured BV2 and modeled ICH in vitro with Hemin, a common hematoma component (Hu et al., 2020; Duan et al., 2021). Cells were collected 24 h later for IP analysis to verify the binding between IL-18 and IL-18 R. In the following, we attempted to explore the potential mechanism of action underlying IL-18/IL-18 R-regulated inflammation. After IP analysis and bioinformatics analysis, we performed stereotactic injection of IL-18 R gene-interfering adeno-associated virus and pharmacological intervention (bumetanide). In this part, mice after viral injection were executed for IF (n = 2) and WB (n = 6) analyses, other mice were randomly divided into 6 groups, including sham group, ICH group, ICH + NC group, ICH + IL-18RKD group, ICH + PBS group, and ICH + bumetanide group. Twenty-four hours after ICH, some mice in each group were subjected to MRI (ICH + NC group, ICH + IL-18RKD group, ICH + PBS group, and ICH + bumetanide group, n = 3) and then were executed to collect brain tissues for WB analyses (n = 6); 10 mice in each group were subjected to behavioral tests. The number of animal subjects was based on previous studies (Wu et al., 2020; Li et al., 2022). All behavioral assessments were performed by two members of the laboratory team, who were blind to the specific situation of the samples.

2.4. Establishment of the experimental ICH model in mice

An experimental ICH model in vivo was established by injection of autologous blood as previous description (Li et al., 2022). Mice were anesthetized with 4% isoflurane, and their anesthetized state were maintained with continuous 2% isoflurane delivery by a mask. Then, mice were fixed in stoelting stereotaxic instrument (Stoelting Co., USA). The median scalp was shaved, sterilized, and a median incision was made using a bone stripper to expose the anterior and sagittal sutures. A circular hole was drilled in the skull, and a microinjector was introduced into the right striatum (0.2 mm anterior, 2.3 mm lateral, and 3.5 mm ventral to the Bregma point) for the infusion of autologous blood. A total volume of 20 μL autologous blood, untreated with anticoagulants, obtained by removing approximately 3 mm from the tail tip, was infused into the striatum at a controlled rate of 2 μL/min through a burr hole. Following the completion of the injection, the microinjector was gradually withdrawn after being held in place for 5 min. Bone wax was applied to seal the bone hole, and the skin incision was disinfected and sutured. The body temperature was maintained at 37.0 ± 0.3 °C during surgery via a temperature regulated heating pad.

2.5. Immunofluorescence (IF) analysis

Mice were anesthetized and the hearts were fixed by perfusion with 4% paraformaldehyde. The brain tissues were dehydrated and embedded in Sakura OCT Compound (USA) embedding agent, and then sectioned using a frozen microtome. Immunofluorescence imaging was focused on the brain around the autologous blood injection site, especially the tissue near the striatum. Different brain slices were co-stained using IL18 (diluted 1:500) or IL18R (diluted 1:500) with corresponding antibodies NeuN (diluted 1:2000), Iba1(diluted 1:1500), and GFAP (diluted 1:2000). As some of the antibodies used were of homologous origin, a double-labeled triple-color multiplex immunofluorescence kit (AFIHC023) from AIFang Bio was employed. The sections were subsequently observed under a fluorescence microscope (Carl Zeiss Co., Ltd, Germany).

2.6. Magnetic resonance imagings (MRI)

MRI was employed to assess hematoma size at 24 h post-ICH, following established protocols. A small-animal MRI system (Bruke Pharmascan 70/16 US, Germany) equipped with a specialized mouse brain coil facilitated image acquisition. Animals were anesthetized with 1.5% isoflurane prior to the procedure, with continuous monitoring of cardiac function using an animal monitoring system. Body core temperature was maintained at 37 °C using a heated pad throughout the procedure. Cerebral hemorrhage volume was assessed using the t2star gre3D sequence, which captured cross-sectional images of the mouse brain at the hemorrhage site, with each section having a uniform thickness. Cross-sections covering all hematoma regions were collected, and the volumes of both the hematomas and corresponding hemispheres were measured using ParaVision 360 software. We then calculated the ratio of hematoma volume to hemisphere volume for each mouse, followed by statistical analysis.

2.7. Western blot (WB) analysis

The brain was removed after irrigation with ice-cold saline and the brain tissue surrounding the hematoma was selected. The volume of the tissue sample (striatum only) was approximately 8 cubic millimeters. Total tissue protein was extracted (12,000 r/min, 5 min, 4 °C) and then quantified using the enhanced BCA Protein Assay Kit (Baiyutian, Shanghai, China). An equal volume of protein (15 μg/lane) was uploaded onto a 10% or 12% SDS-polyacrylamide gel, separated and electrophoretically transferred to a polyvinylidene difluoride (PVDF) membranes (Univ-Bio Co., LTD, Shanghai, China), and blocked for 1 h at room temperature with 5% skimmed milk. β-actin (diluted 1:10,000) was used as a loading control. Next, the membranes were incubated with HRP-conjugated secondary antibodies (Pierce, Rockford, IL, USA) for 1 h. Band signals were then visualized using an Enhanced Chemiluminescence (ECL) Kit (New Cell & Molecular Biotech Co., Ltd, Shanghai, China). Subsequently, protein quantities were analyzed using Image J (NIH, Bethesda, MD, USA, RRID:SCR_003070) and normalized to the loading control.

2.8. Immunoprecipitation (IP)

After washing and activating the protein A agarose beads (Santa Cruz, sc-2003) with CO-IP lysis solution (Beyotime, P0013), the beads were sealed and activated with 2% BSA. Sufficient amount of antibody was then added and the agarose beads were spun on a spinner overnight. On the next day, the agarose beads were washed and extracted protein lysate was added. This mixture is fully incubated on the spinner for 8–10 h to complete protein-antibody binding. The collected agarose beads underwent washing with lysis buffer for three times. Subsequently, the bound proteins were eluted using sample buffer (containing 100 mM Tris-HCl at pH 6.8, 200 mM dithiothreitol, 4% sodium dodecyl sulfate, 0.2% bromochlorophenol blue, and 20% glycerol) through heating at 96 °C for 10 min. The eluates were then collected for WB analysis. The antibodies for IP were rabbit IL- 18 antibody (Proteintech, 10663-1-AP, 4ug) and rabbit NKCC1 antibody (Abcam, ab303518, 3ug).

2.9. Stereotactic injection of adeno-associated virus

In this study, pAAV9-U6-shRNA (IL-18R1)-CMV-EGFP-WPRE and pAAV9-U6-shRNA (NC)-CMV-EGFP-WPRE viruses were purchased from Heyuan Biotechnology Corp., Ltd. (Shanghai, China, catalog number Y29204), and the serotype was Adeno-Associated Virus 9 (AAV9). Viruses were stereotactically injected into the striatum (AP + 0.2 mm; ML + 2.3 mm; DV − 3.5 mm). On the 21st day after injection, all mice were modeled by ICH.

2.10. Stereotactic injection of IL-18BP

IL-18BP was dissolved in normal saline, achieving a final concentration of 50 μg/mL, and was stored at −80 °C. Before inducing intracerebral hemorrhage in the mice, we used a microsyringe to inject 2 μL of the IL-18BP suspension into the striatum (AP + 0.2 mm; ML + 2.3 mm; DV − 3.5 mm) using a stereotactic approach. The control group of mice received the same method of injection with an equivalent volume of normal saline.

2.11. Cell culture

The mouse microglial cell line BV2 (obtained from Sevicebio Biotechnology Co., Wuhan, China, STCC20009) was maintained in DMEM (Gibco GlutaMAX, Thermo Fisher Scientific), supplemented with 1% penicillin/streptomycin (Thermo Fisher Scientific) and 10% fetal bovine serum. The cells were cultured in a 5% CO2 incubator at 37 °C with humidified air. Medium renewal was performed every two days by replacing half of the culture medium.

2.12. Quantitative RT-PCR

Total RNA was extracted from tissues. The specific protocol used has been described previously (Xia et al., 2023). Briefly, the RNA was reverse transcribed into complementary DNA (cDNA) by the specific kits (Hifair® II 1st Strand cDNA Synthesis Kit, YEASEN Biotech Co., Ltd). RT-PCR was conducted with SYBR Green (Roche, Germany) on the 7500 Real-Time PCR system (Applied Biosystems, USA). The primer sequences are as follows: IL-18R1-F: TGGTGGCTGTTTCATTCCTGT; IL-18R1-R: TGGTGGCTGTTTCATTCCTGT; GAPDH-F: CATGGCCTTCCG TGTTCCTA; GAPDH-R: GCCTGCTTCACCACCTTCTT. Relative expression was determined by the $2^{-\Delta\Delta CT}$ method (Livak et al., 2001).

2.13. Bumetanide administration

For bumetanide, an inhibitor of NKCC1, all mice were administered intramuscular injections at a dose of 0.016 mg/kg immediately following the modeling procedure. To ensure consistent drug exposure, a second dose was administered 12 h after the initial injection. This dosing schedule was applied uniformly across both behavioral testing and other experimental groups, including those undergoing western blotting and related analyses.

2.14. Neurobehavioral scores

The impact of ICH on behavioral impairments was evaluated by observing changes in appetite, locomotor activity, and neurological functions in mice, using a scoring system as previously published (Xu et al., 2019). Neurological assessments were performed on at 72 h post-ICH to evaluate behavioral impairments.

2.15. Foot-fault test

Forelimb placement dysfunction was assessed using the foot-fault test (Li et al., 2015). Mice were positioned on an elevated grid surface, placing their paws on the wire while traversing the grid. A foot fault was considered when paws fell between the grid bars. The number of foot faults on both sides was recorded over a 2-min period, and the side difference in foot faults was used for statistical analysis.

2.16. Grip strength test

Grasping strength tests were conducted to measure the grasping strength of the front paws by digital force gauge (YLS-13 A Instrutherm, Shanghai). The animal's front paws were placed on a metal bar connected to the strain gauge. Then, the animal's tail was gently pulled until

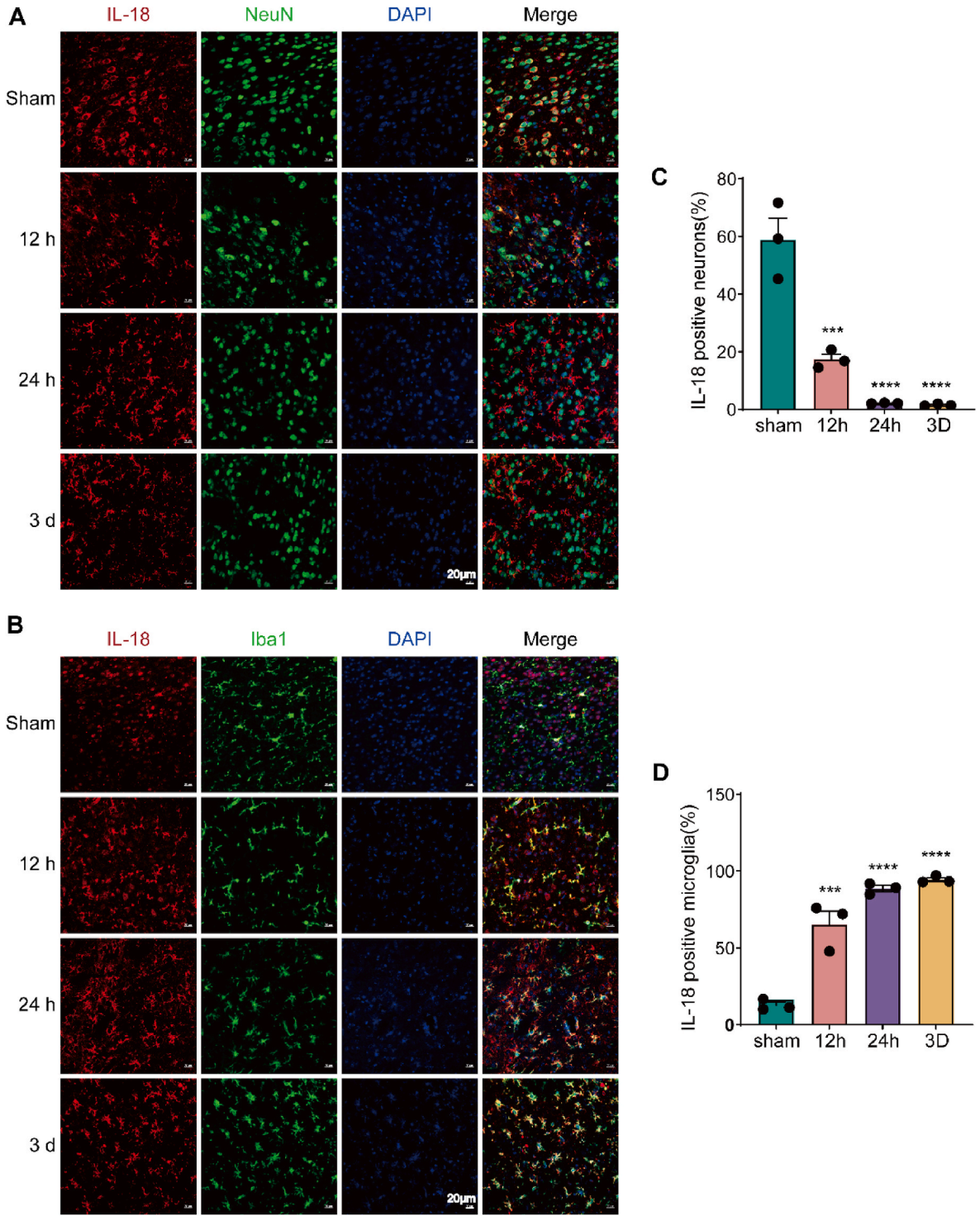

Fig. 1. IL-18 co-localized with neurons and microglia in the striatum in ICH mice. After ICH for different time (12 h, 24 h, and 3d), mouse brains were collected and fixed. Immunofluorescent staining was performed in brain sections (scale bar = 20 μm, N = 3). Nuclei were fluorescently labeled with DAPI (blue). (A) Immunofluorescent staining and the co-localization of IL-18 (red) and NeuN (green) were examined in the striatum of ICH mice at 12 h, 24 h, and 3d. (B) Immunofluorescent staining and the co-localization of IL-18 (red) and Iba1 (green) was examined in the cortex of ICH mice at 24 h, 24 h, and 3d. (C) Quantitative analysis of the number of IL-18 positive neurons. $F(3, 8) = 46.86$, $P < 0.001$, $N = 3$. (D) Quantitative analysis of the number of IL-18 positive microglia. $F(3, 8) = 57.66$, $P < 0.001$, $N = 3$. (For interpretation of the references to color in this figure legend, the reader is referred to the Web version of this article.)

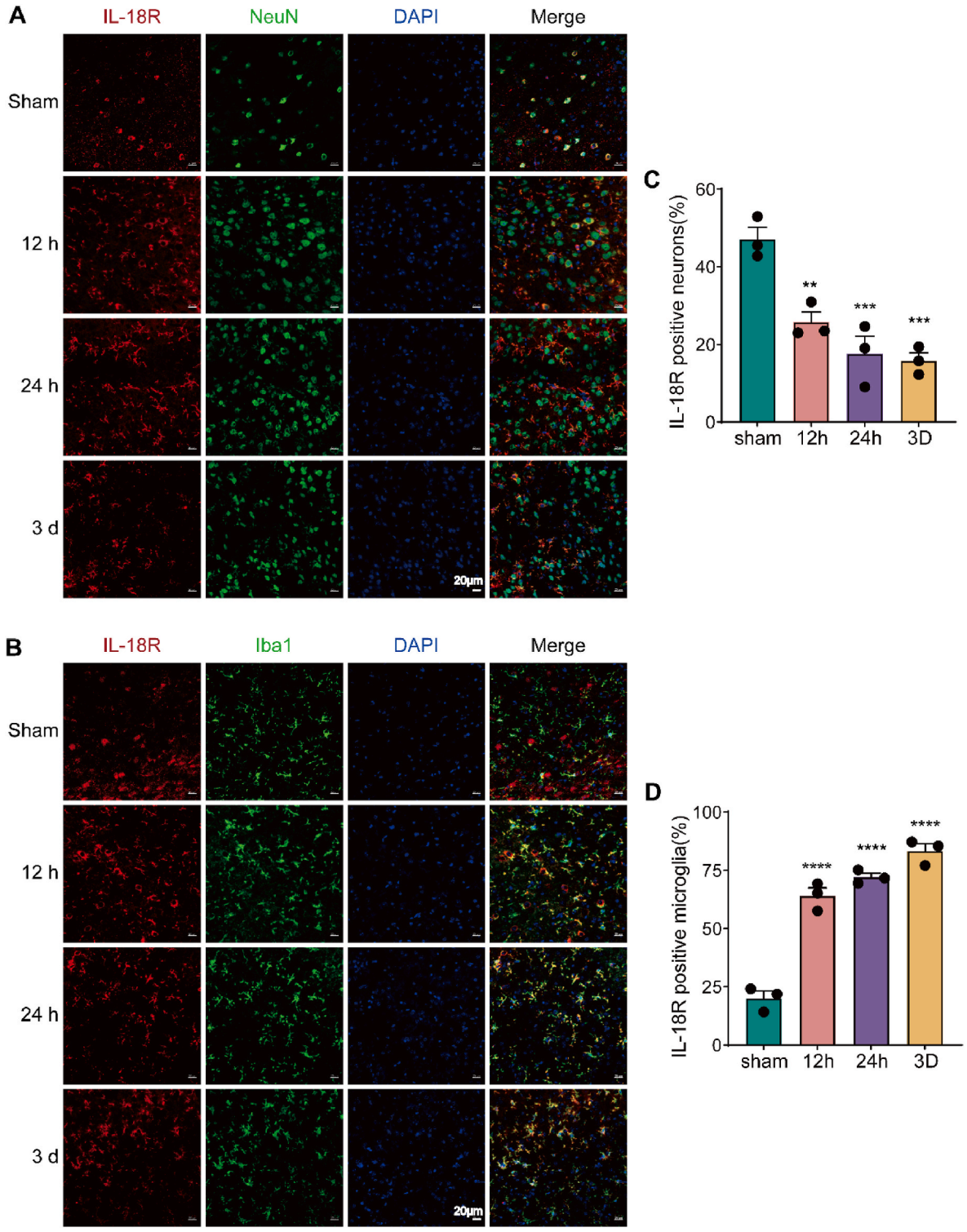

Fig. 2. IL-18 R co-localized with neurons and microglia in the striatum in ICH mice. After ICH for different time (12h, 24 h, and 3d), mouse brains were collected and fixed. Immunofluorescent staining was performed in brain sections (scale bar = 20 μm, N = 3). Nuclei were fluorescently labeled with DAPI (blue). (A) Immunofluorescent staining and the co-localization of IL-18 R (red) and NeuN (green) was examined in the cortex striatum of ICH mice at 12 h, 24 h, and 3d. (B) Immunofluorescent staining and the co-localization of IL-18 R (red) and Iba1 (green) was examined in the cortex striatum of ICH mice at 12 h, 24 h, and 3d. (C) Quantitative analysis of the number of IL-18 positive neurons. $F(3, 8) = 20.19$, $P = 0.004$, $N = 3$. (D) Quantitative analysis of the number of IL-18 positive microglia. $F(3, 8) = 91.74$, $P < 0.001$, $N = 3$. (For interpretation of the references to color in this figure legend, the reader is referred to the Web version of this article.)

it released the metal bar. The values of the three trials were recorded in grams (g) and the average value for each animal was calculated.

2.17. Cylinder test

The cylinder test enables the measurement of the laterality index (Arbaizar-Rovirosa et al., 2023). Mice were placed inside a glass cylinder with an inner diameter of 9.5 cm and a height of 15 cm, designed to encourage vertical exploration of the cylinder walls using their forelimbs. While the mice stood on their hind limbs, the count of initial touches made by the forelimbs against the cylinder wall was recorded over a 10-min period. Counts for left-side, right-side, and bilateral contacts were tallied separately. The asymmetry index for mouse forelimb movement was calculated as the difference between the number of contacts with the affected side and the number of contacts with the healthy side, divided by the total number of initial contacts (comprising affected-side contacts, healthy-side contacts, and simultaneous bilateral contacts).

2.18. Statistics

Continuous variables were checked for the normal distribution assumption by the Shapiro-Wilk test. Data were expressed as mean ± SEM or the median and interquartile range, properly. Two-tailed unpaired Student's t-test was used to compare the differences between the two groups. For group comparisons, one-way ANOVA with Dunnett's post hoc test was used, and for comparisons involving multiple factors, two-way ANOVA with Tukey's post hoc test was applied. Two-way ANOVA with post hoc test was used for differences among groups. The level of significance for these descriptive comparisons was established at 0.05. Statistical analysis was performed with GraphPad Prism version 9.0. The GeneMANIA website (http://genemania.org) was used to predict functionally similar genes of hub genes and construct the PPI network among them (Franz et al., 2018). It can also predict the relationships among functionally similar genes and hub genes, including protein-protein, protein-DNA interactions, pathways, physiological/biochemical reactions, co-expression, and co-localization.

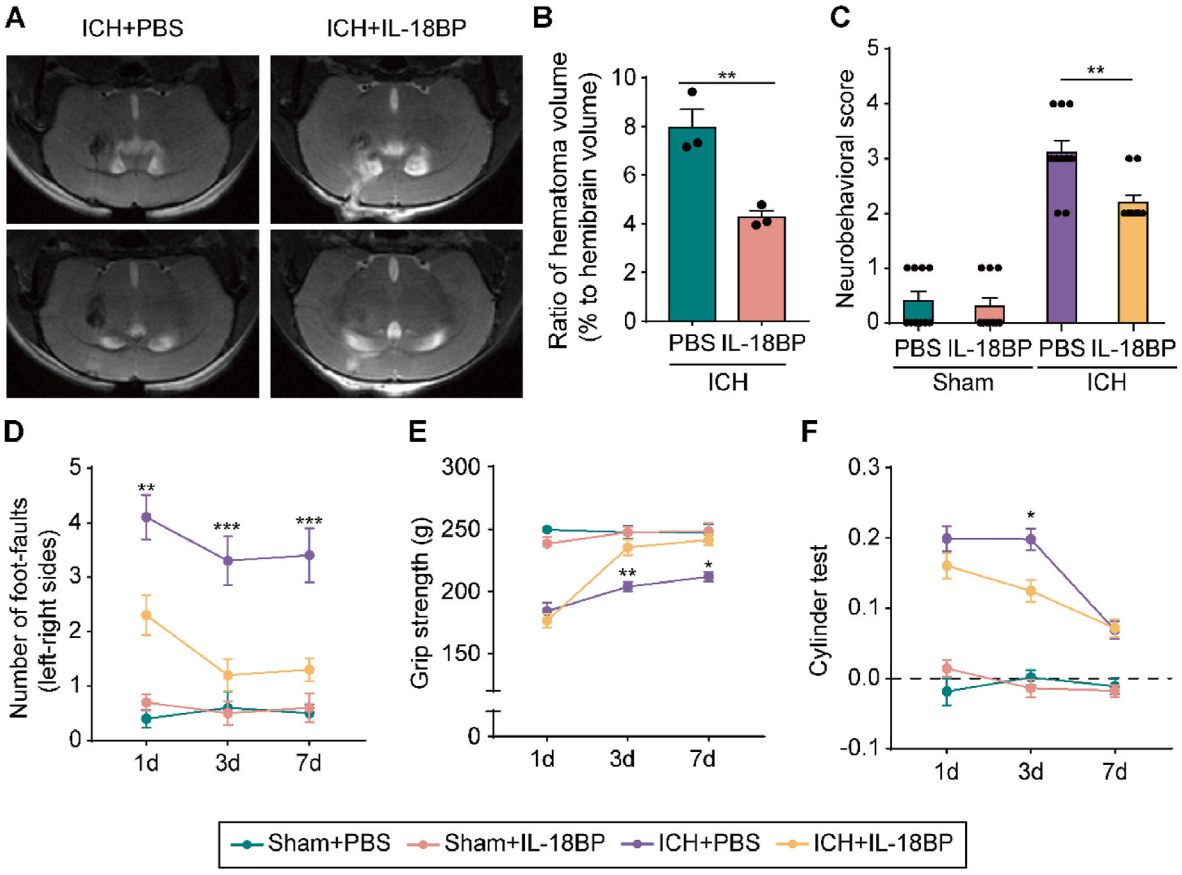

Fig. 3. IL-18BP blocks IL-18 and its receptors from interacting after ICH. (A) Representative T2 MR images (T2WI) of brain at 24 h after ICH in the ICH + PBS group and ICH + IL-18BP group. (B) Quantitative analysis of hematoma size at 24 h after ICH in the ICH + PBS group and ICH + IL-18BP group. F (1, 4) = 22.791, P = 0.008, N = 3. (C) Neurobehavioral scores were evaluated in the Sham + PBS group, Sham + IL-18BP group, ICH + PBS group, and ICH + IL-18BP group at 24 h after ICH. F (3, 36) = 62.18, P < 0.0001, ICH + PBS group vs. ICH + IL-18BP group, P = 0.0045, N = 10. (D) Foot-fault test was examined in the Sham + PBS group, Sham + IL-18BP group, ICH + PBS group, and ICH + IL-18BP group at 1d, 3d, and 7d after ICH. The times of left foot and right foot falling from the grid were recorded. The foot fault times were calculated by left side-right side. F_{row} (2, 108) = 2.790, P = 0.0659; F_{column} (3, 108) = 63.55, P < 0.0001. 1d ICH + PBS vs. 1d ICH + IL-18BP, P = 0.0048; 3 d ICH + PBS vs. 3d ICH + IL-18BP, P = 0.0004; 7d ICH + PBS vs. 7d ICH + IL-18BP, P = 0.0004, N = 10. (E) Grip strength test was examined in the Sham + PBS group, Sham + IL-18BP group, ICH + PBS group, and ICH + IL-18BP group at 1d, 3d, and 7d after ICH. F_{row}(2, 108) = 2.790, P = 0.0659; F_{column}(3, 108) = 63.55, P < 0.0001. 1d ICH + PBS vs. 1d ICH + IL-18BP, P = 0.0048; 3d ICH + PBS vs. 3d ICH + IL-18BP, P = 0.0004; 7d ICH + PBS vs. 7d ICH + IL-18BP, P = 0.0004, N = 10. (F) Cylinder test was examined in the Sham + PBS group, Sham + IL-18BP group, ICH + PBS group, and ICH + IL-18BP group at 1d, 3d, and 7d after ICH. F_{row}(2, 108) = 2.790, P = 0.0659; F_{column}(3, 108) = 63.55, P < 0.0001. 1d ICH + PBS vs. 1d ICH + IL-18BP, P = 0.0048; 3d ICH + PBS vs. 3d ICH + IL-18BP, P = 0.0004; 7d ICH + PBS vs. 7d ICH + IL-18BP, P = 0.0004, N = 10. Data are presented as mean ± SEM. *P < 0.05; **P < 0.01; ***P < 0.001.

3. Results

3.1. IL-18/IL-18 R was secreted from neurons and microglia after ICH

Previous studies have indicated that in a post-stroke depression mouse model, IL-18 is initially released from neurons, followed by a subsequent release from microglia at higher levels (Wu et al., 2020). To further confirm the cellular sources of IL-18 and IL-18 R after ICH, immunofluorescence staining was performed using IL-18 antibody and IL-18 R antibody and cell type marker antibody at different time points after ICH.

IL-18 and neuronal marker NeuN antibodies showed that IL-18 co-localized with NeuN-positive cells at 12–24 h after ICH but not at day 3 (Fig. 1A and C). IL-18 and microglial marker Iba1 antibodies indicated that IL-18 co-localized with Iba1-positive cells at day 3 after ICH but not at 12 h (Fig. 1B and D). IL-18 R expression was similar to IL-18 in neurons. IL-18 R and neuronal marker NeuN antibodies showed that IL-18 R co-localized with NeuN-positive cells at 12–24 h after ICH but not at day 3 (Fig. 2A and C). However, co-localization was seen in IL-18 R and the Iba1-positive cells at different time points (Fig. 2B and D). IL-18, IL-18 R, and astrocytic marker GFAP antibodies showed that IL-18/IL-18 R did not colocalized with GFAP-positive cells at day 1 and day 3 after ICH (Supplemental Figs. 1A–B). The data suggest that IL-18 may be released from neurons (day 1) and subsequently activates microglia at higher levels (day 3), triggering a cascading response. While IL-18 R distribution changes over time on neurons after ICH, microglia could potentially be the target cells for IL-18 action.

3.2. The blockage of endogenous IL-18 by IL-18BP rescued neurological dysfunction after ICH

IL-18BP has been reported to be a high-affinity IL-18 decoy receptor and capable of neutralizing IL-18 bioactivity (Zhou et al., 2020). To further characterize the role of endogenous IL-18 in an experimental ICH model, we injected IL-18BP into the right striatum of mice and examined the associated behaviors. We employed MRI to evaluate the size of cerebral hematoma. Compared with the ICH + PBS group, the size of hematoma was decreased in the ICH + IL-18BP group (Fig. 3A–B, $p < 0.01$). Further behavioral assessment also revealed that the ICH + IL-18BP group exhibited milder neurological impairment compared to the PBS treatment group. In addition to neurological scores (24 h after modeling), we performed the cylinder test, grip strength test and foot-fault test. Neurologic scores were significantly decreased in IL-18BP treated mice (Fig. 3C, $p < 0.01$). In the foot-fault test, IL-18BP reduced motor coordination impairment and decreased lateral differences (Fig. 3D, $p < 0.01$). Consistently, IL-18BP reduced impaired motor function after ICH in the grip test and Cylinder test (Fig. 3E–F, $p < 0.05$). Together, these findings demonstrate that IL-18BP is effective in reducing hematoma volume and alleviating neurological deficits after ICH.

3.3. The interaction of IL-18 and IL-18 R mediated neurological dysfunction after ICH

Further, we detected the alteration of combining strength between IL-18 and IL-18 R after ICH by co-IP. Hemin was applied to establish the ICH model in vitro. Compared to the control group, the binding strength between IL-18 and IL-18 R was enhanced after modeling (Fig. 4A–B). To explore the expression levels of IL-18 R in mouse brain tissues after ICH, WB was employed to detect them in vivo. Our data indicated that IL-18 R protein levels were significantly increased after 12–24 h of ICH compared with those of the sham group (Fig. 4C–D, $p < 0.05$). After that, we performed RT-PCR to assess the mRNA levels of IL-18 R. Consistent with the result of WB, IL-18 R mRNA levels significantly increased in brain tissues of mice after 12–24 h of ICH (Fig. 4E, $p < 0.01$). To further demonstrate the involvement of IL-18 R in neurological impairment after cerebral hemorrhage, we injected IL18R1-interfering adeno-associated viruses or blank vector viruses (NC) into the striatum of C57/BL mice. Injection sites and virus-infected areas were shown in Fig. 4F. WB analysis showed that reduced levels of IL-18 R protein were observed in mice treated with IL18R1-interfering adeno-associated viruses, whereas they were not observed in mice treated with NC virus (Fig. 4G–H, $p < 0.001$). Compared with controls and NC virus-treated mice, hematoma volume was reduced in IL18R1-interfering adeno-associated viruses-treated mice (Fig. 4I–J, $p < 0.05$). In addition, neurologic scores were significantly decreased in IL18R1-interfering adeno-associated viruses-treated mice (Fig. 4K, $p < 0.05$). Similarly, IL18R1-interfering adeno-associated viruses treatment attenuated the neurologic deficits during cylinder test, grip strength test and foot-fault test (Fig. 4L–N, $p < 0.05$). More interestingly, our results showed that IL-18 R knockdown reduced the infiltration of microglia around the hematoma (Fig. 4O–P, $p < 0.05$). Together, these findings demonstrate that IL-18 R deficiency attenuates neurological impairment after ICH in mice.

3.4. IL-18 R deficiency prevented the activation of the NF-κB signaling pathway

To reveal the role of IL-18 R in mouse brain, we constructed Protein-Protein Interaction Networks (PPI) network and extracted key MCODE components (Fig. 5A–B). The results suggested that the interaction between IL-18 and IL-18 R was most closely related to inflammatory responses, cytokine production and activation of the NF-κB signaling pathway. We examined the TLR4/TRAF6/NF-κB signaling pathway, which is recognized as an essential pathway for the release of downstream cytokines (Yang et al., 2020). The expression levels of TLR4 and TRAF6, along with the NF-κB nuclear translocation, were observed to be elevated 24 h post-ICH compared to the sham group, which suggested the activation of the NF-κB pathway (Fig. 5C–G, $p < 0.05$). This effect was inhibited after IL18R1-interfering adeno-associated viruses' treatment (Fig. 5C–G, $p < 0.05$).

3.5. IL-18 induced neurological impairments after ICH by the interaction of IL-18 R with sodium-potassium-chloride co-transporter 1 (NKCC1)

Mature IL-18 is secreted by cells and functions through its receptors (Kaplanski, 2018). However, the precise mechanism by which secreted IL-18 binds to its receptor and induces nerve damage following ICH remains unclear. NKCC1 has been reported to be closely associated with microglial morphology and the regulation of cytokine production (Tóth et al., 2022). Our previous study also suggests the potential formation of a complex or interaction between IL-18 R and NKCC1 within the cell membrane (Wu et al., 2020). In this study, as expected, IL-18 R was detected in immunoprecipitated protein by anti-NKCC1 antibody. The interaction between IL-18 R and NKCC1 was enhanced in the ICH group compared to the sham group (Fig. 6A–B, $p < 0.001$). This further validated the interaction between IL-18 R and NKCC1 after ICH. Meanwhile, recent studies have confirmed that NKCC1 can be implicated in the regulation of microglial ionic homeostasis and inflammatory responses in cerebrovascular disease (Wu et al., 2020; Tóth et al., 2022; Huang et al., 2019). To demonstrate whether NKCC1 is involved in IL-18/IL18 receptor-induced neurological injury after ICH, we intramuscularly injected bumetanide, a specific inhibitor of NKCC1, into ICH-modeled mice at the time of modeling and again at 23 h post-modeling. As can be seen on MRI images, bumetanide injection significantly reduced intracranial hematoma volume (Fig. 6C–D, $p < 0.05$). Also, bumetanide improved neurological function scores compared with the ICH + PBS group (Fig. 6E, $p < 0.01$). Similarly, bumetanide also significantly improved the outcome of cylinder test, grip strength test and foot-fault test in mice after modeling (Fig. 6F–H, $p < 0.05$). Similar to the previous results, our results showed that bumetanide also reduced the infiltration of microglia around the hematoma (Fig. 6I–J, $p < 0.05$). Meanwhile, bumetanide decreased the expression levels of TLR4 and

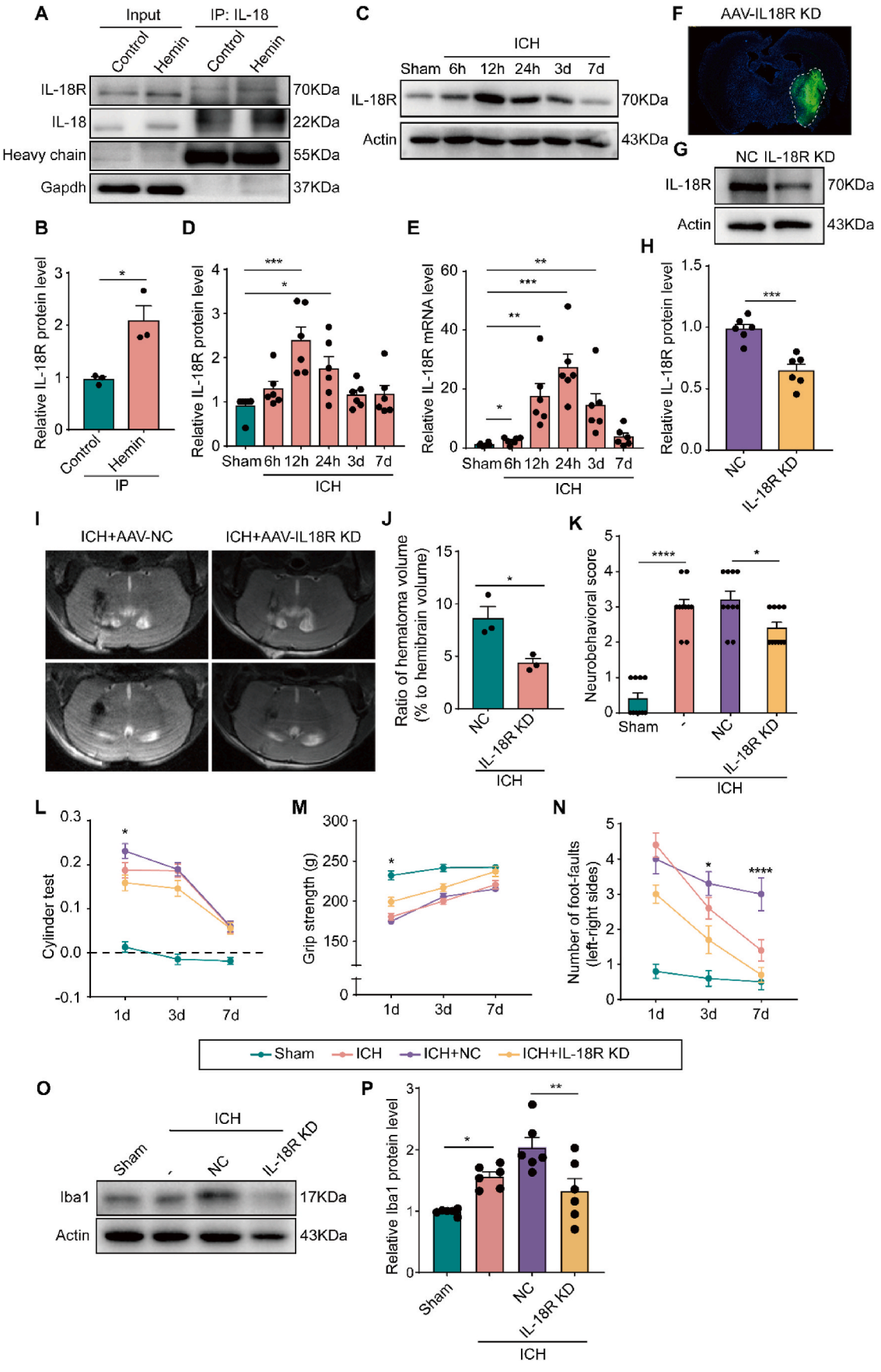

(caption on next page)

Fig. 4. IL-18 R deficiency attenuates neurologic impairment after ICH. (A–B) We cultured BV2 and modeled ICH in vitro with Hemin, then collected cells 24 h later. Co-immunoprecipitation experiment and quantification of the protein levels of IL-18 R were used to show the interaction of IL18 and IL-18 R. (B) F (1, 4) = 14.36, P = 0.0193, N = 3. (C–D) Western blot analysis and quantification of the protein levels of IL-18 R in brain tissues around hematoma at different time points after ICH (6 h, 12 h, 24 h, 3 d, and 7 d). (D) F (5, 30) = 6.747, P = 0.003, N = 6. (E) The mRNA levels of IL-18 R was determined by RT-PCR in brain tissues at different time points after ICH (6 h, 12 h, 24 h, 3 d, and 7 d). F (5, 30) = 11.09, P < 0.0001, N = 6. (F) Packaged virus control (Paav9-U6-shRNA(NC)-CMV-EGFP-WPRE, NC) and pAAV9-U6-shRNA (IL-18R1)-CMV-EGFP-WPRE (AAV-IL18R KD) viruses were injected into the striatum of C57BL/6 mice by a stereotactic method. At 21 d after virus injection, fluorescent microscope photography showed the AAV-expressed IL-18 R KD in the mouse striatum. (G–H) Protein levels of IL-18 R in brain tissues were examined by Western blot analysis in the IL18R1-interfering adeno-associated viruses' group and blank vectors (NC) group at 21 d after virus injection. (H) F (1, 10) = 26.48, P = 0.004, N = 6. (I–J) Representative T2 MR images (T2WI) of brain and quantification of hematoma size at 24 h after ICH in the ICH + NC group and ICH + IL-18RKD group. (J) F (1, 4) = 12.47, P = 0.024, N = 3. (K) Behavioral scores were evaluated in the Sham group, ICH group, ICH + NC group, and ICH + IL-18RKD group at 72 h after ICH. F (3, 36) = 40.92, P < 0.0001; ICH + NC group vs. ICH + IL-18 R KD group, P = 0.0365, N = 10. (L–N) Cylinder test, grip strength test, and foot-fault test were examined in the Sham group, ICH group, ICH + NC group, and ICH + IL-18RKD group at 1 d, 3 d, and 7 d after ICH. (L) F_{row} (2, 108) = 63.67, P < 0.0001; F_{column} (3, 108) = 82.05, P < 0.0001. 1 d ICH + NC vs. 1 d ICH + IL-18 R KD, P = 0.029, N = 10. (M) F_{row} (2, 108) = 41.10, P < 0.0001; F_{column} (3, 108) = 41.32, P < 0.0001. 1 d ICH + NC vs. 1 d ICH + IL-18 R KD, P = 0.038, N = 10. (N) F_{row} (2, 108) = 27.13, P < 0.0001; F_{column} (3, 108) = 44.09, P < 0.0001. 7 d ICH + NC vs. ICH + IL-18 R KD, P < 0.0001, N = 10. (O–P) Protein levels of Iba1 in brain tissues were examined by Western blot analysis in the IL18R1-interfering adeno-associated viruses' group and blank vectors (NC) group at 21 d after virus injection. (P) F (3, 20) = 10.39, P = 0.0002, N = 6. Data are presented as mean ± SEM. *P < 0.05; **P < 0.01; ***P < 0.001; ****P < 0.0001.

TRAF6 as well as the NF-κB nuclear translocation at 24 h after ICH compared with the control group (Fig. 6K–O, $p < 0.05$). These suggest that bumetanide inhibits the inflammatory response after ICH and rescues nerve injury. All these findings indicate that IL-18 R is likely involved in the regulation of microglia-mediated inflammatory injury by forming a complex with NKCC1 or interacting in the cell membrane.

4. Discussion

In our previous studies, we have observed that IL-18 is involved in activating microglia to enhance the inflammatory response, confirming the important role of IL-18 in brain injury after ICH. However, the mechanisms by which IL-18 specifically activates microglia after hemorrhagic stroke are poorly understood. In this study, IL-18 and IL-18 R were predominantly secreted by neurons during the first 12–24 h after ICH, with microglia becoming the primary source of secretion thereafter. IL-18BP can rescue neurological deficits after ICH by blocking endogenous IL-18. Meanwhile, the expression level of IL-18 R increased following ICH, accompanied by an increase in the binding affinity between IL-18 R and IL-18. Furthermore, IL-18 R deficiency attenuated neurological impairment and subsequent activation of inflammatory pathways after ICH in mice. Finally, we demonstrated that IL-18-induced neurologic injury after ICH may be mediated by the interaction between IL18R and NKCC1. In summary, our study suggests that activation of IL-18 R on non-microglial cells plays a key role in microglial activation, inflammatory responses, hematoma formation, and related behavioral deficits following ICH, highlighting the IL-18/IL-18R/NKCC1 pathway as a potential therapeutic target for secondary brain injury treatment.

IL-18, as a pro-inflammatory cytokine, is thought to play a crucial role in cerebrovascular disease and alexithymia (Du et al., 2022; Hao et al., 2019). Increased levels of IL-18 are associated with enhanced expression of other markers on inflammation and hemostasis, including IL-6, C-reactive protein, fibrinogen, viscosity, factor VIII, and fibrin D-dimer (Ihim et al., 2022). However, data on the specific role of IL-18 in ICH and related mechanisms of actions are still very limited. Generally, IL-18 is secreted from neurons only in certain nuclei in the absence of external stimuli (Kuwahara-Otani et al., 2017). Some studies, in the one hand, have shown that IL-18 is mainly secreted by microglia in excitotoxic or ischemia-induced brain injury (Jia et al., 2023; Jeon et al., 2008). In the other hand, a time lag between IL-18 in neurons and microglia was observed in mice after the MCAO model and spatial restraint stress (Wu et al., 2020). In the present study, we observed the distribution of IL-18 and its receptor at different time points after modeling, and again different degrees of time lag were observed. We inferred that the rapid initial IL-18 secretion by neurons after ICH induced microglial cell activation and facilitated the continued release of IL-18 from microglia. Meanwhile, both neurons and microglial cells expressed IL-18 R, but the expression of neuronal IL-18 R was mainly concentrated in the 24 h after modeling, whereas it persisted in microglial cells for a longer period of time.

In clinical studies, cerebrospinal fluid levels of IL-18 were especially elevated in the group of SAH patients and in preterm infants with posthemorrhagic hydrocephalus (Schmitz et al., 2007; Lv et al., 2018). These elevated levels were positively correlated with adverse outcomes (Schmitz et al., 2007; Lv et al., 2018). Our previous study also confirmed that IL-18 tends to increase after ICH, and IL-18 KO exerted a neuroprotective effect after ICH and alleviated IL-18-induced microglial infiltration around the hematoma (Li et al., 2022). In the present study, both immunofluorescence and WB verified this. Interestingly, not only IL-18 but also IL-18 R expression was increased in the brain tissue surrounding the hematoma after ICH. Meanwhile, the binding of IL-18 and its receptor could be found to be enhanced after ICH by in vitro experiments. Through pharmacological and viral interventions, we investigated the role of IL-18 and its receptor in mediating inflammatory injury after cerebral hemorrhage. In the AAV-mediated regulation of IL-18, due to the extremely low infection efficiency of AAV in microglia, this approach primarily targeted neurons, astrocytes, and other IL-18 R-expressing cells that could be infected (Lv et al., 2018; Maes et al., 2019). Based on previous immunofluorescence results, we preliminarily determined that this manipulation mainly influences the interaction between IL-18 and its receptor on neurons within the first 12–24 h after injury. This supports the conclusion that the IL-18/IL-18 R interaction mediates the early inflammatory cascade triggered by cerebral hemorrhage.

NKCC1 functions as a membrane protein primarily responsible for transporting Na^+, K^+, and Cl^- ions into the cell, thereby maintaining intracellular Cl^- concentration (Lam et al., 2023). In our previous studies, IL-18 could mediate depressive behavior in post-stroke depression through the IL-18R/NKCC1 pathway (Wu et al., 2020). This is also supported by a recent study suggesting that Na-Cl cotransporter proteins are necessary for the normal function of IL-18 (Wang et al., 2015). In the current study, we verified the interaction between IL-18 R and NKCC1 after ICH by immunoprecipitation, suggesting that NKCC1 may mediate IL-18-induced neuroinflammatory injury after cerebral hemorrhage via IL-18 R. In human studies, inhibition of NKCC1 by bumetanide (a specific inhibitor of NKCC1) has been considered for use in treating Alzheimer's disease (Boyarko et al., 2023). We employed bumetanide as an NKCC1 inhibitor to treat post-modeling mice to further validate the role of NKCC1 after ICH. The results suggested that it could rescue the neuroinflammatory injury after ICH in mice, which supports the involvement of NKCC1 as an ion transport protein in the IL-18/IL-18 R pathway.

However, there are some limitations to our study. Specifically, we used only male mice in our experiments, a decision informed by previous research indicating that estrogen confers cerebral protection in brain

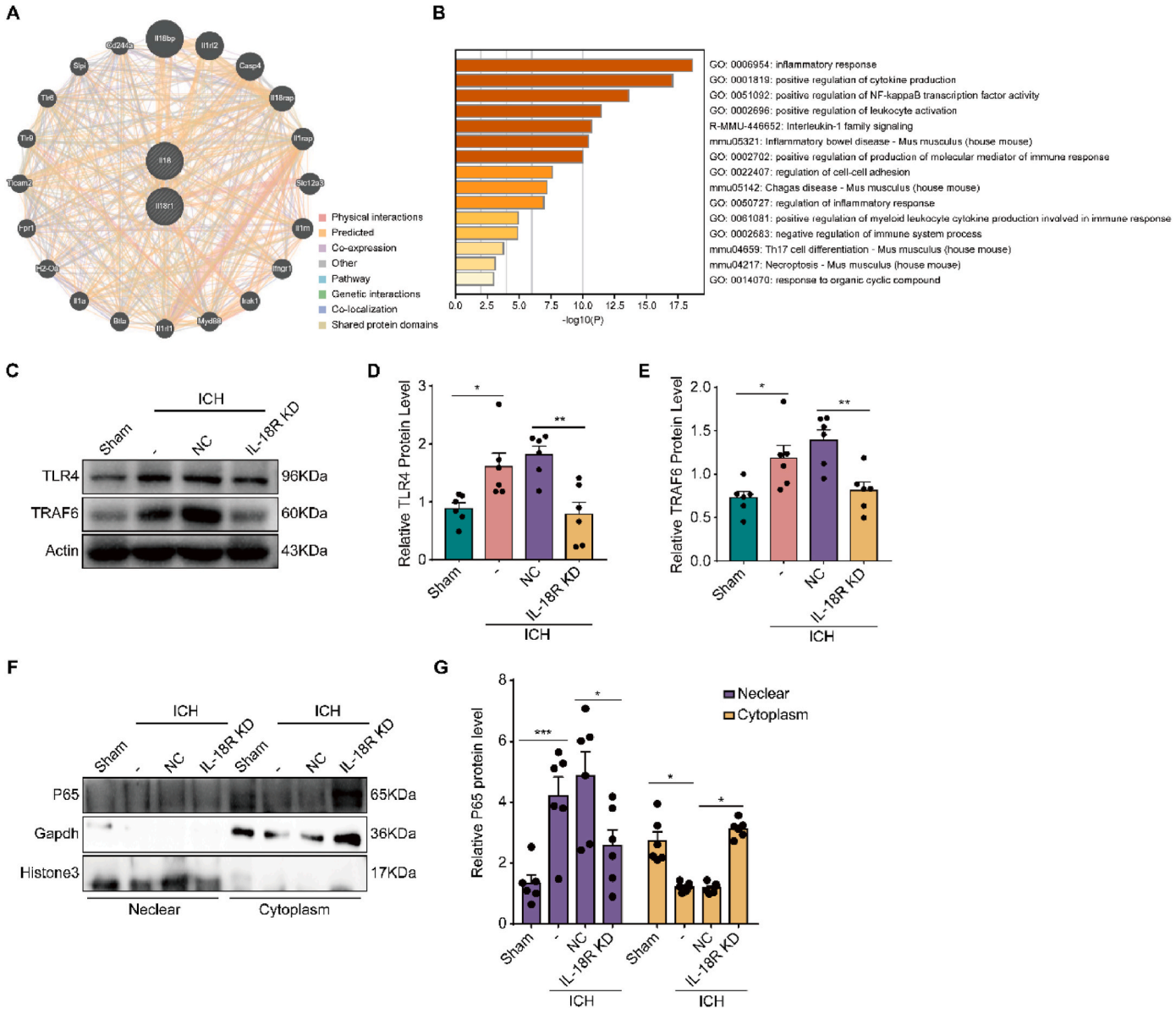

Fig. 5. IL-18 R deficiency prevents activation of subsequent signaling pathways. (A) Protein-Protein Interaction Networks (PPI) networkby identifying genes functionally similar to IL-18/IL-18 R (GeneMANIA). (B) Key MCODE components were extracted and subjected to Gene Ontology (GO) analysis using Metascape, which used genes identified by GeneMANIA. (C–E) Western blot analysis and quantification of the protein levels of TLR4 and TRAF6 in brain tissues around hematoma among the Sham group, ICH group, ICH + NC group, and ICH + IL-18RKD group at 24 h after ICH. (D) $F(3, 20) = 7.994$, $P = 0.0011$, $N = 6$. (E) $F(3, 20) = 7.820$, $P = 0.0012$, $N = 6$. (F–G) After separating nuclear and cytoplasmic proteins in brain tissues surrounding the hematoma, Western blot analysis and quantification of the protein levels of NF-κB in the nucleus and cytoplasm among the Sham group, ICH group, ICH + NC group, and ICH + IL-18RKD group at 24 h after ICH. (G) $F_{row}(3, 40) = 2.063$, $P = 0.1205$, $F_{column}(1, 40) = 15.04$, $P = 0.0004$, $N = 6$. Data are presented as mean ± SEM. $^{*}P < 0.05$; $^{**}P < 0.01$; $^{***}P < 0.001$.

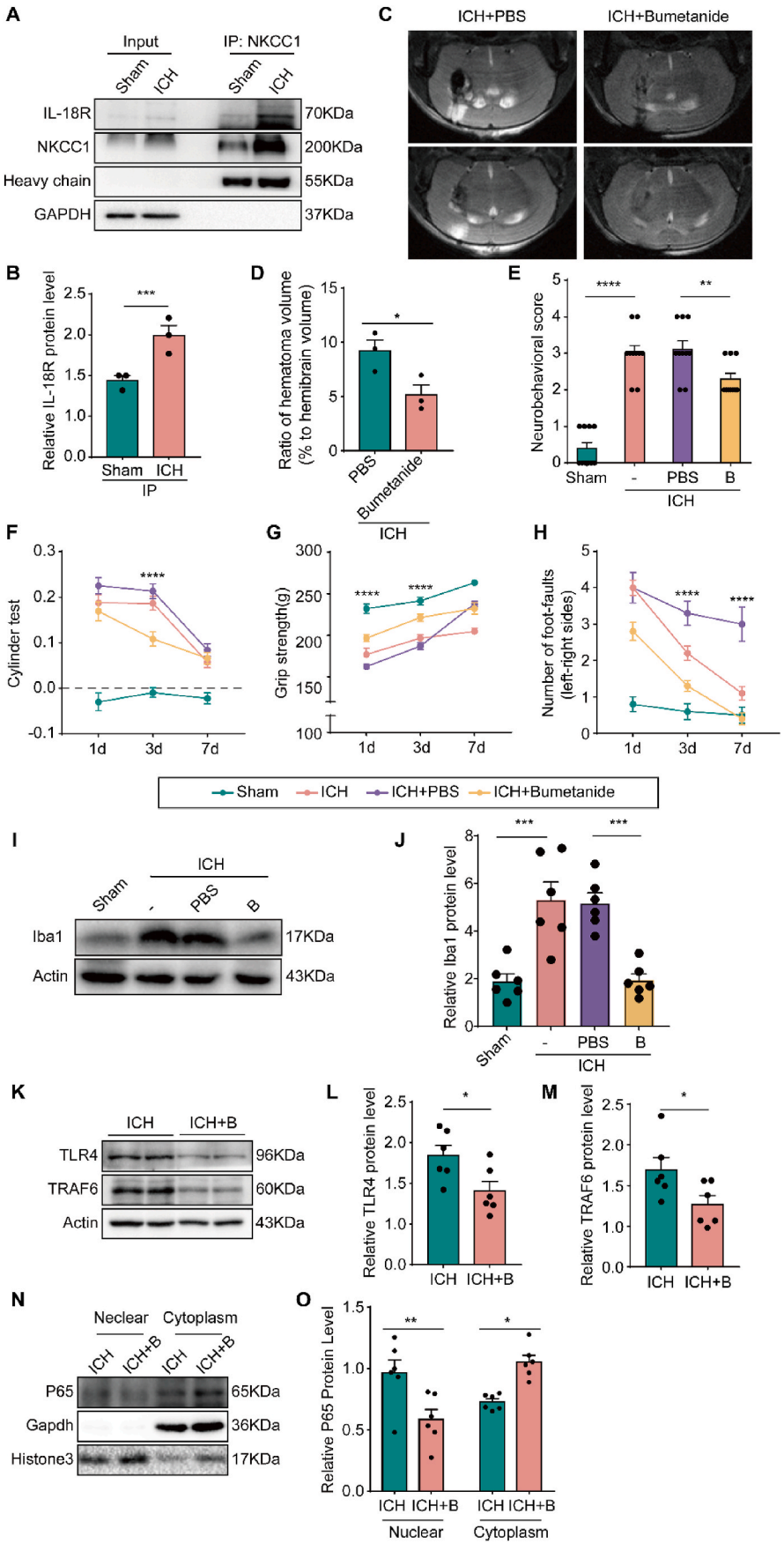

(caption on next page)

Fig. 6. IL-18 exacerbates post-ICH neurological impairments by interacting with IL-18 R and NKCC1. (A–B) Co-immunoprecipitation experiment and quantification of the protein levels of IL-18 R in brain tissues around hematoma at 24 h after ICH were used to show the interaction of IL18R and NKCC1. (B) F(1,4) = 78.76, P = 0.0009, N = 3. (C–D) Representative T2 MR images (T2WI) of brain and quantification of hematoma size at 24 h after ICH in the ICH + PBS group and ICH + bumetanide group. (D) F(1,4) = 8.51, P = 0.043, N = 3. (E) Behavioral scores were evaluated in the Sham group, ICH group, ICH + PBS group, and ICH + bumetanide group at 24 h after ICH. F (3, 36) = 42.09, P < 0.0001, N = 10. (F–H) Cylinder test, grip strength test, and foot-fault test were examined in the Sham group, ICH group, ICH + PBS group, and ICH + bumetanide group at 1 d, 3 d, and 7 d after ICH. (F) F_{row} (2, 108) = 40.17, P < 0.0001; F_{column} (3, 108) = 90.51, P < 0.0001. 3 d ICH + PBS vs. 3 d ICH + Bumetanide, P < 0.0001, N = 10. (G) F_{row} (2, 108) = 82.51, P < 0.0001; F_{column} (3, 108) = 81.40, P < 0.0001. 1 d ICH + PBS vs. 1 d ICH + Bumetanide, P < 0.0001; 3 d ICH + PBS vs. 3 d ICH + Bumetanide, P < 0.0001, N = 10. (H) F_{row} (2, 108) = 38.05, P < 0.0001; F_{column} (3, 108) = 59.45, P < 0.0001. 3 d ICH + PBS vs. 3 d ICH + Bumetanide, P < 0.0001; 7 d ICH + PBS vs. 7 d ICH + Bumetanide, P < 0.0001, N = 10. (I–J) Western blot analysis and quantification of the protein levels of Iba1 in brain tissues around hematoma between ICH group and ICH + bumetanide group at 24 h after ICH. (J) F (3, 20) = 15.66, P < 0.0001; N = 6. (K–M) Western blot analysis and quantification of the protein levels of TLR4 and TRAF6 in brain tissues around hematoma between ICH group and ICH + bumetanide group at 24 h after ICH. (L) F (1, 10) = 6.25, P = 0.0304; N = 6. (M) F (1, 10) = 5.28, P = 0.045, N = 6. (N–O) After separating nuclear and cytoplasmic proteins in brain tissues surrounding the hematoma, Western blot analysis and quantification of the protein levels of NF-κB in the nucleus and cytoplasm between the ICH group and ICH + bumetanide group at 24 h after ICH. (O) F_{row} (1, 20) = 0.1259, P = 0.7265; F_{column} (1, 20) = 2.478, P = 0.1311. ICH vs. ICH + B (Nuclear), P = 0.0089; ICH vs. ICH + B (Cytoplasm), P = 0.0267. N = 6. Data are presented as mean ± SEM. *P < 0.05; **P < 0.01; ***P < 0.001; ****P < 0.0001.

injury models, which may lead to different immune responses compared to males. (Xiao et al., 2021; Nakamura et al., 2005; Auriat et al., 2005). Although this approach is consistent with many existing studies, it does not fully represent the broader epidemiological data on ICH. Female mice also demonstrate notable neuroimmune responses to ICH, and the potential influence of testosterone, which varies between individuals and during various times of the day, on ICH outcomes and IL-18/IL-18 R expression is a significant consideration (Goldman et al., 2017). Future research should address these limitations by incorporating female and aged mice to achieve a more comprehensive understanding of ICH pathophysiology and the role of sex hormones in neuroinflammatory responses. Additionally, our study only explored the mechanism of the IL-18/IL-18 R-regulated cascade response triggered by early-stage inflammatory factors after ICH and did not delve further into its role in long-term recovery or other processes, such as immune cell polarization, which remain to be further elucidated.

In conclusion, previous studies have established a connection between IL-18 and ICH. In this study, we demonstrated that increased IL-18 levels in perihematoma brain tissue mediated neuroinflammatory injury in a mouse ICH model by activating IL18R/NKCC1 signaling. Therefore, targeting IL-18 or its signaling pathways would be a promising therapeutic strategy for the prevention and treatment of ICH.

CRediT authorship contribution statement

Beibei Xu: Writing – original draft, Investigation, Data curation. **Hao Li:** Writing – original draft, Investigation, Formal analysis, Data curation. **He Zheng:** Validation, Data curation. **Zhongyu Gao:** Software. **Zhigang Miao:** Project administration, Methodology, Investigation. **Xingshun Xu:** Writing – review & editing, Conceptualization. **Hao Yang:** Writing – review & editing, Project administration, Conceptualization. **Yi Yang:** Writing – review & editing, Writing – original draft, Funding acquisition, Data curation, Conceptualization.

Ethics approval and consent to participate

This study involving animals was reviewed and approved by the Institutional Review Board of The First Affiliated Hospital of Soochow University. The experiments comply with the current laws of the country in which they were performed.

Availability of data and materials

Original data of the present study are available from the corresponding author upon reasonable request.

Funding

This work was supported by grants from the National Natural Science Foundation of China (82201446) and the Natural Science Foundation of Jiangsu Province of China (BK20220249).

Declaration of competing interest

On behalf of all authors, the corresponding author states that there is no conflict of interest.

Appendix A. Supplementary data

Supplementary data to this article can be found online at https://doi.org/10.1016/j.bbih.2024.100890.

Data availability

Data will be made available on request.

References

Arbaizar-Rovirosa, M., et al., 2023. Aged lipid-laden microglia display impaired responses to stroke. EMBO Mol. Med. 15 (2), e17175.
Auriat, A., et al., 2005. 17beta-Estradiol pretreatment reduces bleeding and brain injury after intracerebral hemorrhagic stroke in male rats. J. Cerebr. Blood Flow Metabol. 25 (2), 247–256.
Bao, J., et al., 2020. Rapamycin protects chondrocytes against IL-18-induced apoptosis and ameliorates rat osteoarthritis. Aging (Albany NY) 12 (6), 5152–5167.
Boyarko, B., et al., 2023. Evaluation of bumetanide as a potential therapeutic agent for Alzheimer's disease. Front. Pharmacol. 14, 1190402.
Dinarello, C.A., 2001. Novel targets for interleukin 18 binding protein. Ann. Rheum. Dis. 60 (Suppl. 3), 18–24. Suppl 3.
Ding, Y., et al., 2020. Annexin A1 attenuates neuroinflammation through FPR2/p38/COX-2 pathway after intracerebral hemorrhage in male mice. J. Neurosci. Res. 98 (1), 168–178.
Du, X., et al., 2022. Peripheral Interleukin-18 is negatively correlated with abnormal brain activity in patients with depression: a resting-state fMRI study. BMC Psychiatr. 22 (1), 531.
Duan, L., et al., 2021. Baicalin inhibits ferroptosis in intracerebral hemorrhage. Front. Pharmacol. 12, 629379.
Franz, M., et al., 2018. GeneMANIA update 2018. Nucleic Acids Res. 46 (W1), W60–w64.
Goldman, A.L., et al., 2017. A reappraisal of testosterone's binding in circulation: physiological and clinical implications. Endocr. Rev. 38 (4), 302–324.
Hao, Y., et al., 2019. Increased interleukin-18 level contributes to the development and severity of ischemic stroke. Aging (Albany NY) 11 (18), 7457–7472.
Hu, L., et al., 2020. MicroRNA-152 attenuates neuroinflammation in intracerebral hemorrhage by inhibiting thioredoxin interacting protein (TXNIP)-mediated NLRP3 inflammasome activation. Int. Immunopharm. 80, 106141.
Huang, H., et al., 2019. The WNK-SPAK/OSR1 kinases and the cation-chloride cotransporters as therapeutic targets for neurological diseases. Aging Dis 10 (3), 626–636.
Ihim, S.A., et al., 2022. Interleukin-18 cytokine in immunity, inflammation, and autoimmunity: biological role in induction, regulation, and treatment. Front. Immunol. 13, 919973.
Jeon, G.S., et al., 2008. Glial expression of interleukin-18 and its receptor after excitotoxic damage in the mouse hippocampus. Neurochem. Res. 33 (1), 179–184.
Jia, X., et al., 2023. Association of interleukin-6 and interleukin-18 with cardiovascular disease in older adults: atherosclerosis Risk in Communities study. Eur J Prev Cardiol 30 (16), 1731–1740.
Kaplanski, G., 2018. Interleukin-18: biological properties and role in disease pathogenesis. Immunol. Rev. 281 (1), 138–153.
Kilkenny, C., et al., 2011. Animal research: reporting in vivo experiments–the ARRIVE guidelines. J. Cerebr. Blood Flow Metabol. 31 (4), 991–993.

Kuwahara-Otani, S., et al., 2017. Interleukin-18 and its receptor are expressed in gonadotropin-releasing hormone neurons of mouse and rat forebrain. Neurosci. Lett. 650, 33–37.
Lam, P., et al., 2023. Cation-chloride cotransporters KCC2 and NKCC1 as therapeutic targets in neurological and neuropsychiatric disorders. Molecules 28 (3).
Li, X., et al., 2015. Inhibition of connexin43 improves functional recovery after ischemic brain injury in neonatal rats. Glia 63 (9), 1553–1567.
Li, H., et al., 2022. Interleukin-18 mediated inflammatory brain injury after intracerebral hemorrhage in male mice. J. Neurosci. Res. 100 (6), 1359–1369.
Livak, K.J., Schmittgen, T.D., 2001. Analysis of relative gene expression data using real-time quantitative PCR and the 2(-Delta Delta C(T)) Method. Methods 25 (4), 402–408.
Lv, S.Y., et al., 2018. Levels of interleukin-1β, interleukin-18, and tumor necrosis factor-α in cerebrospinal fluid of aneurysmal subarachnoid hemorrhage patients may Be predictors of early brain injury and clinical prognosis. World Neurosurg 111, e362–e373.
Maes, M.E., et al., 2019. Targeting microglia with lentivirus and AAV: recent advances and remaining challenges. Neurosci. Lett. 707, 134310.
Magid-Bernstein, J., et al., 2022. Cerebral hemorrhage: pathophysiology, treatment, and future directions. Circ. Res. 130 (8), 1204–1229.
Nakamura, T., et al., 2005. Estrogen therapy for experimental intracerebral hemorrhage in rats. J. Neurosurg. 103 (1), 97–103.
Schmitz, T., et al., 2007. Interleukin-1beta, interleukin-18, and interferon-gamma expression in the cerebrospinal fluid of premature infants with posthemorrhagic hydrocephalus–markers of white matter damage? Pediatr. Res. 61 (6), 722–726.
Sukhanov, S., et al., 2021. The SGLT2 inhibitor Empagliflozin attenuates interleukin-17A-induced human aortic smooth muscle cell proliferation and migration by targeting TRAF3IP2/ROS/NLRP3/Caspase-1-dependent IL-1β and IL-18 secretion. Cell. Signal. 77, 109825.
Tang, X., et al., 2020. Activation of PPAR-β/δ attenuates brain injury by suppressing inflammation and apoptosis in a collagenase-induced intracerebral hemorrhage mouse model. Neurochem. Res. 45 (4), 837–850.
Tóth, K., et al., 2022. The NKCC1 ion transporter modulates microglial phenotype and inflammatory response to brain injury in a cell-autonomous manner. PLoS Biol. 20 (1), e3001526.
Tu, W.J., Wang, L.D., 2023. China stroke surveillance report 2021. Mil Med Res 10 (1), 33.
Wang, J., et al., 2015. Interleukin 18 function in atherosclerosis is mediated by the interleukin 18 receptor and the Na-Cl co-transporter. Nat. Med. 21 (7), 820–826.
Wu, D., et al., 2020. Interleukin-18 from neurons and microglia mediates depressive behaviors in mice with post-stroke depression. Brain Behav. Immun. 88, 411–420.
Xia, M., et al., 2023. GID complex regulates the differentiation of neural stem cells by destabilizing TET2. Front. Med. 17 (6), 1204–1218.
Xiao, H., et al., 2021. 17β-Estradiol attenuates intracerebral hemorrhage-induced blood-brain barrier injury and oxidative stress through SRC3-mediated PI3K/akt signaling pathway in a mouse model. ASN Neuro 13, 17590914211038443.
Xu, H., et al., 2019. GATA-4 regulates neuronal apoptosis after intracerebral hemorrhage via the NF-κB/Bax/Caspase-3 pathway both in vivo and in vitro. Exp. Neurol. 315, 21–31.
Yang, Y., et al., 2020. Luteolin alleviates neuroinflammation via downregulating the TLR4/TRAF6/NF-κB pathway after intracerebral hemorrhage. Biomed. Pharmacother. 126, 110044.
Zhang, H., et al., 2018. Role of IL-18 in atopic asthma is determined by balance of IL-18/IL-18BP/IL-18R. J. Cell Mol. Med. 22 (1), 354–373.
Zhou, T., et al., 2020. IL-18BP is a secreted immune checkpoint and barrier to IL-18 immunotherapy. Nature 583 (7817), 609–614.